Available online at www.sciencedirect.com
SCIENCE DIRECT®
ELSEVIER
Synthetic Metals 146 (2004) 329–334
SYNTHETIC METALS
www.elsevier.com/locate/synmet

Tetracene-based organic light-emitting transistors: optoelectronic properties and electron injection mechanism

C. Santato[a], R. Capelli[a], M.A. Loi[a], M. Murgia[a], F. Cicoira[a], V.A.L. Roy[a], P. Stallinga[a,1], R. Zamboni[a], C. Rost[b], S.F. Karg[b], M. Muccini[a,*]

[a] *Istituto per lo Studio dei Materiali Nanostrutturati—CNR, via P. Gobetti 101, 40129 Bologna, Italy*
[b] *IBM-ZRL, Säumerstrasse 4, CH-8803 Rüschlikon, Switzerland*

Available online 1 October 2004

Abstract

Optoelectronic properties of light-emitting field-effect transistors (LETs) fabricated on bottom-contact transistor structures using a tetracene film as charge-transport and light-emitting material are investigated. Electroluminescence generation and transistor current are correlated, and the bias dependence of the LETs external quantum efficiency is determined. The device's performance degrade rapidly upon gate biasing. The effect is attributed to charge trapping, which can be prevented by operating the devices in pulsed mode.

A model for the electron injection mechanism in a p-type organic transistor is proposed. On the basis of this model, electrical and optical characteristics, as well as the dependence of the external quantum efficiency on drain- and gate-bias, are well reproduced.
© 2004 Elsevier B.V. All rights reserved.

Keywords: Field effect transistor; Optoelectronics; Change injection

1. Introduction

Organic materials have been proved successful for use as active layers in electronic and optoelectronic devices such as light emitting diodes (OLEDs), thin film transistors (OTFTs) and photovoltaic cells (OPVs). Device performance and reliability have been radically improved since early prototype reports [1–4], allowing OLEDs to enter the market and OTFTs to reach charge mobility comparable to that of amorphous silicon transistors [5–7]. Recently, organic light-emitting (field-effect) transistors (OLETs) have been demonstrated [8]. OLETs represent a relevant novel opportunity to investigate fundamental optoelectronic properties of organic thin films, and to overcome some of the constrains posed by the existing vertically-stacked light-emitting devices. The higher charge carrier mobility for OTFTs, if compared to organic and polymer LEDs (of the order of 10^{-5} cm^2/(V s) under dc operation [9]), should result in lower exciton quenching by charge carriers in OLETs than in OLEDs. The three electrodes device structure of OLETs allows, in principle, to better control injection and currents of electrons and holes to minimize unbalanced mobility and enhance exciton density. Furthermore, taking advantage of the gate electrode bias, the location of the exciton recombination region can be controlled.

In this work, the correlation between electroluminescence and transistor current in recently discovered tetracene-based LETs is investigated. The degradation of the device performances upon device operation is studied and demonstrated to be prevented by pulsed mode gate bias. The light generation mechanism is also investigated. A hypothesis on the driving force and mechanism for electron injection from Au into tetracene was formulated and, on this basis, an analytical model able to describe the light and current outputs is provided.

2. Experimental

The FET structure employed in this study is reported in Fig. 1. Two types of substrates have been considered. The first type is fabricated by first evaporating contact pads formed

* Corresponding author. Tel.: +39 051 6398521; fax: +39 051 6398540.
E-mail address: M.Muccini@ism.bo.cmz.it (M. Muccini).
[1] Permanent address: Universidade do Algarve, FCT 8000 Faro, Portugal.

0379-6779/$ – see front matter © 2004 Elsevier B.V. All rights reserved.
doi:10.1016/j.synthmet.2004.08.028

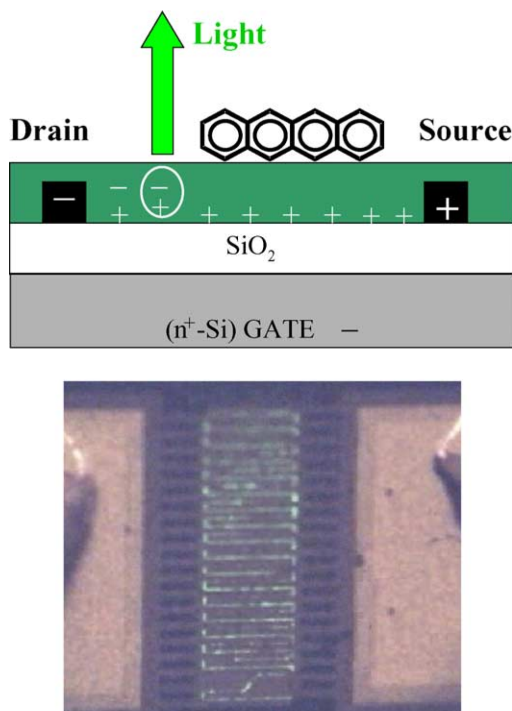

Fig. 1. Structure of the organic light-emitting transistors fabricated on SiO_2/*n*-Si substrates (top). Light is generated by recombination of holes and electrons injected into the transistor channel by source and drain contacts, respectively. Example of a working OLET with W_c/L_c = 200,000/5 (μm/μm) (bottom).

by 10 nm thick Ti/W adhesion layer and 200 nm thick Au layer on 100 nm thick SiO_2 (gate dielectric with capacitance of 3.45×10^{-8} F/cm^2) thermally grown on *n*-Si substrate (gate electrode). Source and drain electrodes were formed by sputtering 15 nm thick Au layer. Patterning was done by a lithographic process. Ultra-thin Au electrodes with no adhesion layer ensured charge injection to occur from gold, and prevented shadow effects when subliming the organic ultrathin film. Gold electrode profiles were checked with AFM to have smooth slopes and to be highly regular along the entire channel width. Channel lengths (L_c) and widths (W_c) varied in the range 2–20 μm and 100–1048 μm, respectively. The second type of substrates was fabricated employing 290 nm thick SiO_2 (oxide capacitance of 1.8×10^{-8} F/cm^2) thermally grown on *n*-Si substrate, respectively acting as gate dielectric and gate electrode. A thin chromium adhesive layer was deposited on the oxide surface before 50 nm thick Au was deposited. After that, source and drain interdigitated electrodes were photolithographically patterned. W_c was 20 cm and L_c was 15 μm.

The substrate surface was treated with octadecyl-trichlorosilane (OTS) to improve substrate coverage and film homogeneity [10]. Tetracene films with thickness in the range from 20 to 50 nm were sublimed in high vacuum conditions with the substrate kept at room temperature. OLETs were then placed in a probe station inside a calibrated integrating sphere, where light detection was achieved through a pre-amplified photomultiplier [11]. Simultaneous current and electroluminescence measurements were systematically performed in vacuum at room temperature both in dc and pulsed mode.

Leakage current through the oxide could result in electron injection into tetracene followed by light generation. To rule out any contribution of the leakage current to the light generation, some of the experiments were performed using an ad hoc experimental configuration where the same bias was applied to drain and gate with respect to source and currents were measured at the drain. In this way, strictly no current between drain and gate is possible, and the electrical characteristics measured at the drain can be exclusively attributed to the two-dimensional transistor channel.

3. Results and discussion

Tetracene LETs behave as p-channel unipolar transistors. No electron current was ever detected in these devices [8]. Fig. 2 shows the light output intensity and the drain current as the $V_{DS} = V_G$ is scanned from 0 to −40 V. The onset of the electroluminescence is at higher voltage than the onset of the drain current and the electroluminescence intensity increases faster than the current at higher voltages. Fig. 2 reveals the non-linear correlation between light and current. The external quantum efficiency (EQE) of the device, defined as the number of emitted photons per charge carrier, is well described by a quadratic function in the $V_{DS} = V_G$ applied voltage (inset Fig. 2).

Fig. 3 shows hysteresis loops for drain current and electroluminescence intensity obtained by scanning the $V_{DS} = V_G$ voltage in dc mode from 0 to −40 V and back. Both the current and light backward curves fall below the forward ones due to a significant increase of the threshold gate voltage upon device operation [12]. Charge trapping was iden-

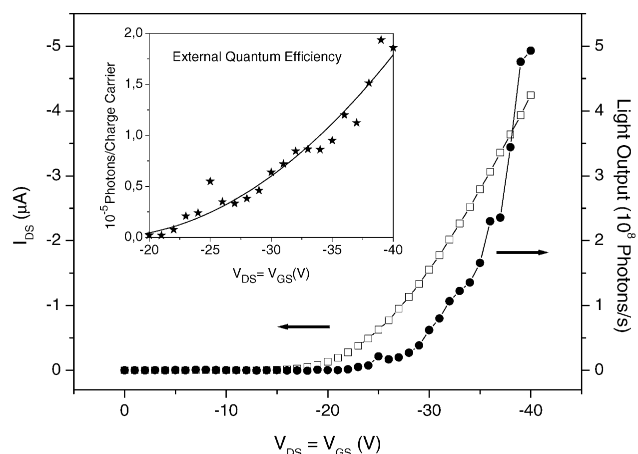

Fig. 2. Drain current (□) and electroluminescence intensity (●) as a function of $V_{DS} = V_G$. The inset shows the external quantum efficiency measured for $V_{DS} = V_{GS}$ in the range from −20 to −40 V (the continuous line is a fit to the experimental data with a quadratic function of the applied voltage). Transistor with W_c/L_c = 1048/5 (μm/μm).

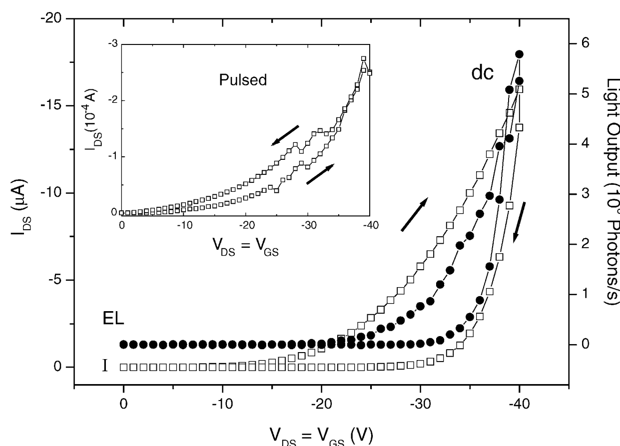

Fig. 3. Hysteresis loops for drain current (□) and electroluminescence intensity (●) measured in dc mode. The inset shows the same drain current measurement performed in pulsed mode with ms voltage pulses. Transistor with W_c/L_c = 1048/5 (μm/μm).

tified as the possible origin of the increase of threshold gate voltage during device operation. To avoid charge trapping, pulsed voltages can be applied to the device. Indeed, pulsing the gate with ms voltage pulses changes the device response, i.e. the backward current curve is now superimposed or possibly higher than the forward one (see inset of Fig. 3). No similar effect was observed pulsing the drain voltage. These results indicate that the gate bias plays a major role in inducing charge trapping. The effect of charge trapping on current and electroluminescence was studied by transient measurements where a constant voltage was applied to gate and drain whilst current and light were measured as a function of time. Fig. 4 shows transient measurements for constant V_{DS} = V_G = −40 V. The different decay of current with respect to electroluminescence suggests that different processes are responsible for charge flow and light generation. Inset of Fig. 4 also

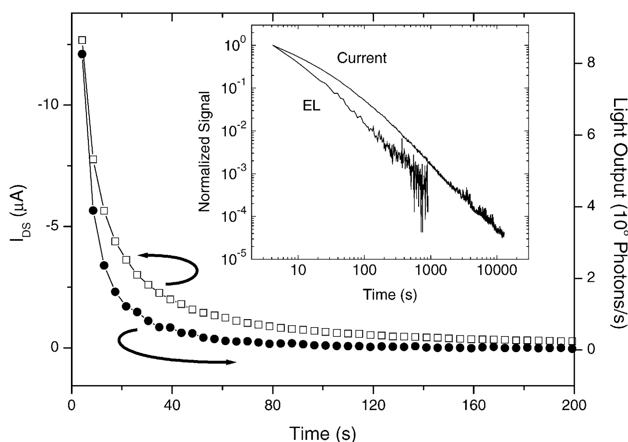

Fig. 4. Transient measurements of drain current (□) and electroluminescence intensity (●) for constant V_{DS} = V_G = −40 V. The inset shows the log–log plot extended to 10^4 s. Transistor with W_c/L_c = 1048/5 (μm/μm).

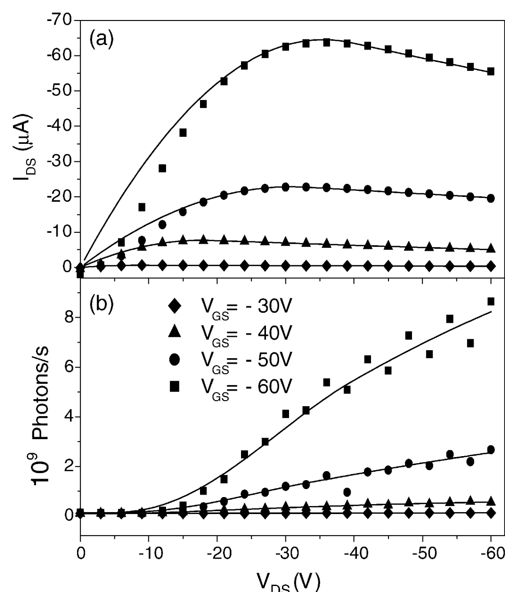

Fig. 5. (a) Electrical output characteristics (symbols) and correspondent simulations (continuous lines). The mobility μ_h extracted from the experimental curves and used as parameter in the fitting is 1×10^{-4}, 2.6×10^{-4}, 2.6×10^{-4}, and 5×10^{-4} cm^2/(V s) for V_{GS} −30, −40, −50, and −60 V, respectively. Transistor with W_c/L_c = 200,000/5 (μm/μm). (b) Experimental (symbols) and simulated (continuous lines) optical output characteristics, corresponding to Fig. 5a.Transistor with W_c/L_c = 200,000/5 (μm/μm).

shows that both current and electroluminescence transients are not described by a single exponential decay. The electroluminescence decreases faster than the current and after a few hundreds seconds is below the detection limit. Although the decay of the current is slower, it also approaches the noise level after 10^4 s. The nature and exact location of charge trap states in organic devices is still a matter of debate. Trap states have originally been observed in amorphous silicon TFTs [13] well before their investigation in organic and polymeric TFTs [14]. Work is in progress to investigate deeply the nature and energetics of traps in organic light-emitting transistors.

Figs. 5a and 6a show the standard output and transfer characteristics of the device [15]. A clear effect of metal–organic contact resistance is displayed in the I_D–V_{DS} curves at low drain-voltage [16–18]. A decreasing drain current instead of the typical saturation is observed for higher drain-voltages. This effect was attributed to the increase of the gate voltage threshold during device operation. Charge mobility deduced from the transfer curves reported in Fig. 6a is one order of magnitude higher with respect to that obtained from the output curves of Fig. 5a. Such a difference is caused by the different gate bias mode employed to record the output curves (constant mode) and the transfer ones (staircase mode). Indeed, the major role played by the gate bias in inducing the charge trapping was already underlined. The optical response of OLETs corresponding to the electrical output and transfer characteristics are shown in Figs. 5b and 6b, respectively.

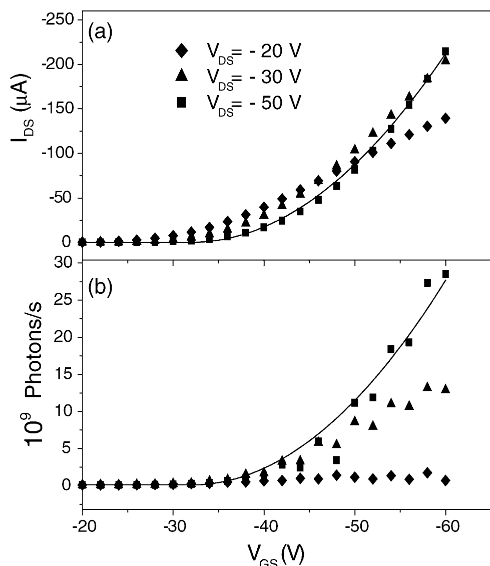

Fig. 6. (a) Electrical transfer characteristics (symbols) and correspondent simulations (continuous lines). The mobility μ_h extracted from the experimental curves and used as parameter in the fitting is 2×10^{-3}, 3.3×10^{-3}, and 4.4×10^{-3} $cm^2/(V\,s)$ for V_{GS} −20, −30, and −50 V, respectively. Transistor with W_c/L_c = 200,000/5 (μm/μm). (b) Experimental (symbols) and simulated (continuous lines) optical transfer characteristics, corresponding to Fig. 6a.Transistor with W_c/L_c = 200,000/5 (μm/μm).

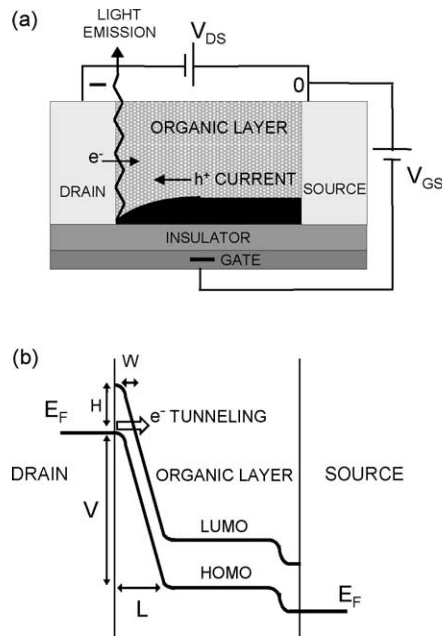

Fig. 7. (a) Working principle of OLET device. The main electronic processes taking place when the device is operated in standard p-type mode are indicated. (b) Energy levels diagram showing the mechanism for electron injection from gold into the organic material at the drain electrode.

4. Modeling OLETs

4.1. The model

The open question concerning the working mechanism of OLETs is the electron injection from gold into tetracene, which is energetically strongly unfavourable. The non-ohmic contact at the metal–organic interface is shown by the non-linear increase of I_D [16–18] at low V_{DS} in Fig. 5a. Due to this contact barrier, there is a potential drop near the source and drain electrodes. The specific features of this voltage drop depend on the nature of the metal–organic interface. The proposed model assumes that the voltage drop causes a distortion of the HOMO–LUMO levels of the organic material, near the metal–organic interface, determining the conditions for the tunneling of electrons from drain into the LUMO level of the organic material.

Fig. 7a shows the schematic representation of the main electronic processes occurring in a working OLET device. The gate bias induces hole accumulation in the transistor channel. Hole current flows towards the drain, which is negatively biased with respect to the source. Together with the direct injection of electrons from drain into the HOMO level of tetracene, which leads to a purely non-radiative process, the injection of electrons via tunnelling into the LUMO level can also take place. Injected electrons have a high probability to interact with positively charged tetracene molecules to form excitons, which can then give rise to light emission. Once excitons are formed they are subject to all intramolecular and intermolecular processes, which determine the detected light intensity [19,20]. These processes include the molecular radiative recombination, the exciton-charge carrier interaction and exciton-metal interaction. For simplicity, in our model we consider the intrinsic molecular light-emission efficiency, and group all the extrinsic and intermolecular effects in a rescaling parameter Q_E.

Fig. 7b schematically represents the effect of the voltage drop on the electron injection barrier near the metal–organic interface. The barrier becomes triangular-like with a height (H) equal to the HOMO–LUMO gap and a width (W) inversely proportional to V_{DS}. W is directly proportional to L, i.e. to the extension of the region over which the potential drops at the drain. L is a phenomenological parameter and depends exclusively on the nature of the metal–organic interface. Its value is deduced from the fitting of the experimental electroluminescence output characteristics. We anticipate here that values of L ranging between 3 and 15 nm were obtained.

The analytical equations used to describe the number of electron–hole pairs formed in the channel ($N_{e–h}$), the hole current (I_D) [15,21], the electron injection tunneling probability (P_t) [22,23] and the number of emitted photons (N_{phs}) are given below.

$$N_{e-h} = \frac{I_D(V_{DS}, V_{GS})}{e} P_t(V_{DS}, \Delta E_e) \tag{1}$$

where ΔE_e is the energy distribution of electrons in the gold metal around the Fermi energy level, and I_D and P_t are de-

scribed by the following equations:

$$I_D = \begin{cases} \frac{W_C \mu_h C_{OX}}{L_C}\left[(V_{GS} - V_T)V_{DS} - \frac{1}{2}V_{DS}^2\right], & V_{DS} < V_{GS} - V_T \\ \frac{W_C \mu_h C_{OX}}{2L_C}\left[(V_{GS} - V_T)^2\right], & V_{DS} \geq V_{GS} - V_T \end{cases} \quad (2)$$

$$\begin{cases} P_t = \frac{aH}{eW}e^{-8\pi W\sqrt{2mH}/3h} \\ H = E_{LUMO} - E_{HOMO} - \Delta E_e \\ W = H\frac{L}{V_{DS}} \end{cases} \quad (3)$$

$$N_{Phs} = Q_E\, N_{e\text{–}h}(V_{DS}, V_{GS}) \quad (4)$$

W_c, L_c, C_{ox} and μ_h are the channel width, channel length, oxide capacitance and hole mobility of the OLET device, respectively. The gate-voltage threshold (V_T) is considered to change linearly during device operation in agreement with the experimental observations (see previous section).

The overall trend of the simulated curves arises straightforwardly from the equations using the experimental W_c, L_c, and C_{ox}. Fine tuning of the simulations is done adjusting the values of μ_h and V_T in agreement with the experimental I_D.

4.2. Simulating the electrical and optical characteristics

Figs. 5a and 6a show the OLETs output and transfer characteristics, respectively, with their correspondent simulations. The effect of metal–organic contact barrier shown in the experimental I_D–V_{DS} curves (Fig. 5a) at low drain-voltage has not been considered explicitly in the model, and therefore simulations do not reproduce the S-shape behaviour of the curves at low voltage. The decreasing drain current for higher drain-voltages in Fig. 5a is well described in the correspondent simulations by inclusion of a linear increase of V_T. Consistently with this result, Fig. 8 shows that both for drain current and electroluminescence there is an increase of the gate-voltage threshold of about 10 V upon a cycled measurement, which is reproduced with good accuracy by the correspondent simulation.

Simulations of electroluminescence were performed with the same parameters used to model the current. The drain-voltage onset for light emission is independent of the gate (provided the gate is above its own threshold) in agreement with the hypothesis that it is exclusively dependent on the nature of the metal–organic interface. Fig. 5 shows that at high drain-voltages the current slightly decreases, while the light intensity continues to rise. This can be explained as follows. Since electron–hole recombination depends on the density of holes close to the drain, the number of emitted photons is expected to be proportional to the hole current. We expect also that by increasing the drain-voltage, the electroluminescence intensity would increase more than the drain current because the tunneling barrier depends on V_{DS}. In addition, in the transfer characteristics, by sweeping the gate-voltage at a constant drain-voltage (Fig. 6), both current and light emission intensity steadily increase if the gate is above its threshold. Indeed, the gate-voltage determines the drain current, but does not directly influence the electron injection. A deeper insight on the electron injection process is provided by the dependence of the external quantum efficiency (EQE)

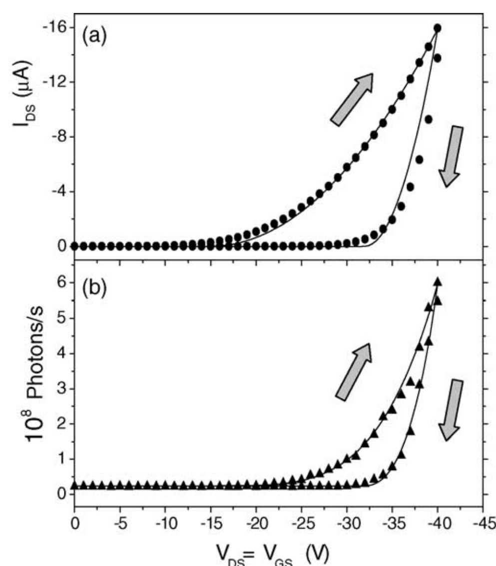

Fig. 8. (a) Experimental (symbols) and simulated (continuous lines) hysteresis loops for drain current. Hysteresis is due to an increase of the gate-voltage threshold during device operation. Transistor with W_c/L_c = 1048/5 (μm/μm). (b) Experimental (symbols) and simulated (continuous lines) hysteresis loops for electroluminescence intensity corresponding to Fig. 8a.Transistor with W_c/L_c = 1048/5 (μm/μm).

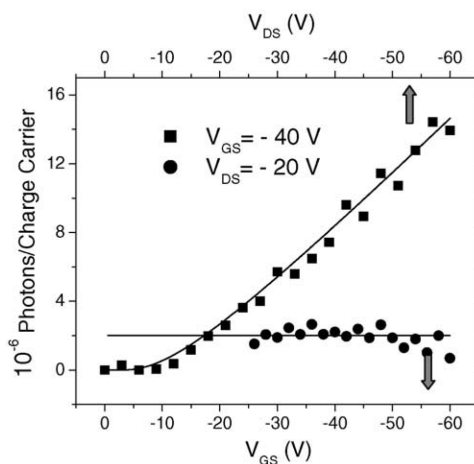

Fig. 9. Experimental (symbols) and simulated (continuous lines) external quantum efficiency as a function of the V_{GS} (●) and of V_{DS} (■). Transistor with W_c/L_c = 200,000/5 (μm/μm).

on the applied gate and drain voltages. In the proposed model, EQE is proportional to the tunneling probability (Eq. (3)) as easily deduced from Eq. (1). P_t depends non-linearly on V_{DS} and is independent on V_{GS}. Fig. 9 reports EQE versus V_{GS} and versus V_{DS} and the correspondent simulations. EQE depends on V_{DS}, whilst it does not depend on V_{GS}. The good agreement between the model and these experiments is a confirmation of the tunnelling hypothesis.

5. Conclusions

Optoelectronic properties of tetracene-based light-emitting transistors were investigated. Device performances degradation upon device operation was attributed to gate voltage-induced hole trapping. Pulsed gate voltage operation mode prevented the trapping. The crucial topic of energetically unfavourable electron injection from Au contact into tetracene was investigated. An analytical model of the device working mechanism was proposed based on electron injection via a tunneling process enabled by the non-ohmic contact between the Au drain electrode and the organic material. Despite the simplified approach, the model reproduces the optoelectronic characteristics of the device, including the drain and gate voltage dependence of the external quantum efficiency. The understanding of the fundamental electronic processes constitutes the know-how platform necessary to realize ambipolar organic light-emitting transistors.

Acknowledgements

The authors acknowledge the EU-IST-FET program under project IST-33057 (ILO) for financial support, and are grateful to P. Heremans, H. von Seggern, R. Ziessel and all the other members of the ILO consortium for stimulating discussions. S. De Jonge and S. De Vusser from IMEC provided Au patterned Si/SiO_2 substrates. V.A.L. Roy is grateful to Fondazione del Monte di Bologna e Ravenna for support.

References

[1] C.W. Tang, S.A. Van Slyke, Appl. Phys. Lett. 51 (1987) 913.
[2] J.H. Burroughes, D.D.C. Bradley, A.R. Brown, R.N. Marks, K. Mackay, R.H. Friend, P.L. Burns, A.B. Holmes, Nature 347 (1990) 539.
[3] F. Garnier, F.Z. Peng, G. Horowitz, D. Fichou, Adv. Mater. 2 (1990) 592.
[4] P. Ostoja, G. Guerri, S. Rossini, M. Servidori, C. Taliani, R. Zamboni, Synth. Met. 54 (1993) 447.
[5] A. Dodabalapur, L. Torsi, H.E. Katz, Science 268 (1995) 270.
[6] Sirringhaus, N. Tessler, R.H. Friend, Science 280 (1998) 1741.
[7] S.F. Nelson, Y.Y. Lin, D.J. Gundlach, T.N. Jackson, Appl. Phys. Lett. 72 (1998) 1854.
[8] A. Hepp, H. Heil, W. Weise, M. Ahles, R. Schmechel, H. von Seggern, Phys. Rev. Lett. 91 (2003) 157406.
[9] N. Tessler, D.J. Pinner, V. Cleave, D.S. Thomas, G. Yahioglu, P. Le Barny, R.H. Friend, Appl. Phys. Lett. 74 (1999) 2764.
[10] F. Cicoira, et al., submitted.
[11] P. Mei, M. Murgia, C. Taliani, E. Lunedei, M. Muccini, J. Appl. Phys. 88 (2000) 5158.
[12] H.L. Gomes, P. Stallinga, F. Dinelli, M. Murgia, F. Biscarini, D.M. de Leeuw, T. Muck, J. Geurts, L.W. Molenkamp, V. Wagner, Appl. Phys. Lett. 84 (2004) 1.
[13] M.J. Powell, Appl. Phys. Lett. 43 (1983) 597.
[14] M. Matters, D.M. de Leeuw, P.T. Herwig, A.R. Brown, Synth. Metals 102 (1999) 998.
[15] S.M. Sze, Physics of Semiconductor Devices, Wiley, 1981.
[16] L. Torsi, A. Dodabalapur, E. Katz, J. Appl. Phys. 78 (1995) 1088.
[17] P.V. Necliudov, M.S. Shur, D.J. Gundlach, T.N. Jackson, J. Appl. Phys. 88 (2000) 6594.
[18] J. Zaumseil, K.W. Baldwin, J.A. Rogers, J. Appl. Phys. 93 (2003) 6117.
[19] M. Pope, C.E. Swenberg, Electronic Processes in Organic Crystals, Clarendon Press, Oxford, 1982.
[20] M.A. Baldo, R.J. Holmes, S.R. Forrest, Phys. Rev. B 66 (2002) 35321.
[21] G. Horowitz, Semiconducting Polymers Chemistry, in: Physiscs and Engineering, Wiley–VCH, 2000.
[22] W. Franz, Ann. Phys. 11 (1952) 17.
[23] J. Kalinowski, J. Phys. D: Appl. Phys. 32 (1999) R179.